

High-throughput descriptor for predicting potential topological insulators in the tetradymite family

Guohua Cao¹, Huijun Liu^{1,*}, Runhai Ouyang², Carlos Mera Acosta², Luca M. Ghiringhelli²,
Zizhen Zhou¹, Matthias Scheffler², Christian Carbogno^{2,†}, Zhenyu Zhang^{3,‡}

¹ *Key Laboratory of Artificial Micro- and Nano-Structures of Ministry of Education and School of Physics and Technology, Wuhan University, Wuhan 430072, China*

² *Fritz-Haber-Institut der Max-Planck-Gesellschaft, Faradayweg 4-6, 14195 Berlin-Dahlem, Germany*

³ *International Center for Quantum Design of Functional Materials (ICQD), Hefei National Laboratory for Physical Sciences at the Microscale, and Synergetic Innovation Center of Quantum Information and Quantum Physics, University of Science and Technology of China, Hefei, Anhui 230026, China*

Abstract Discovery of topological insulators remains a challenge because it is usually laborious, high cost, and time consuming. High-throughput computational prescreening is an effective way to reduce the set of candidate systems. Herein, based on compressed sensing technique, we derive an optimized two-dimensional descriptor which can quickly predict potential topological insulators in the tetradymite family. With only two kinds of fundamental constants of the constituent elements (the atomic number and the electronegativity) as input features, the proposed descriptor effectively classifies topological insulators and normal insulators from a training data containing 230 tetradymite compounds. The predicative accuracy as high as 97% demonstrates that the descriptor really capture the essential nature of topological insulators, and can be further used to fast screen other potential topological insulators beyond the input dataset.

* Corresponding author. Electronic mail: pahlj@whu.edu.cn

† Corresponding author. Electronic mail: carbogno@fhi-berlin.mpg.de

‡ Corresponding author. Electronic mail: zhangzy@ustc.edu.cn

1. Introduction

Topological insulators (TIs) are a new class of quantum materials with insulating bulk and metallic surface/edge state protected by time-reversal symmetry [1-4]. These nontrivial states have a spin helical massless Dirac structure, and hence hold promising application potentials in spintronics and quantum computation devices [5-8]. To date, various TIs have been studied theoretically and/or experimentally, such as binary tetradymite Bi_2Te_3 [9,10], ternary chalcogenide TlBiSe_2 [11,12], hexagonal pnictide CaAgAs [13], and etc. In general, the experimental discoveries of new TIs are limited by time-consuming procedures of synthesis. On the theoretical side, the identifications of topological natures are usually complex, which cannot be detected through a local order parameter. Therefore, more efficient techniques are needed to accelerate materials discovery and design process, such as high-throughput screening and big data analytics (e.g., data mining, machine learning and compressed sensing) [14-16]. In an earlier study, a high-throughput descriptor was developed for predicting new TIs, given by the variational ratio of spin-orbit distortion versus non-spin-orbit derivative strain [17]. More recently, symmetry-based indicators of band topology were applied to search topological materials in 230 space groups [18]. In practice, however, these approaches still need to do detailed electronic structure calculations from first-principles. On the other side, data mining technique has been successfully applied to search stable nitride perovskites [19], bulk topological insulators [20], and organic Dirac-line materials [21]. In addition, machine learning method has also been used to study phase transitions in conventional systems [22-27], topological phase transitions [28-32], gravitational wave analysis [33, 34], black hole detection [35] and formation energy of elpasolite crystals [36]. Nevertheless, for learning target material properties as employing these big data analytics approaches, the physical insight of the descriptive parameters (often called descriptor) is somehow less clear, and the causality of the learned descriptor-property relation is still uncertain. In a recent study using statistical learning theory, Ghiringhelli *et al.* proposed an approach to find meaningful descriptors that can illustrate actuating mechanisms of a certain property [37]. With the help of compressed sensing technique, Ouyang *et al.* [38]

subsequently developed a more systematic methodology to tackle this issue, as implemented in the so-called SISO code (sure independence screening and sparsifying operator). It is thus reasonable to expect that a physically meaningful descriptor optimized by SISO could accelerate materials discovery in TIs.

Binary tetradymites including Bi_2Te_3 , Bi_2Se_3 and Sb_2Te_3 are typical TIs with larger band gaps and non-dissipative topologically protected surface states [9, 10]. Successively, their ternary derivatives $\text{Sb}_2\text{Te}_2\text{S}$ [39], $(\text{Bi}_x\text{Sb}_{1-x})_2\text{Te}_3$ [40], $\text{Sb}_2\text{Te}_2\text{Se}$ [41], and $\text{Bi}_2(\text{Se}_x\text{Te}_{1-x})_3$ [42] were extensively investigated to adjust the position of the Dirac cone and meanwhile to increase the band gap as much as possible. In fact, the tetradymite compounds can be obtained by randomly combining group-VA elements (As, Sb and Bi) with group-VIA elements (S, Se and Te). It is thus natural to ask if topological nature exists in many other possible ternary, quaternary, quintuple or hexahydroxy tetradymites, which is less known so far.

In this article, using only the atomic number and electronegativity of the constituent atoms as input features, a two-dimensional (2D) descriptor is proposed to effectively classify TIs and normal insulators (NIs) in a training data of 230 tetradymites. The cross-validation indicates that the optimized descriptor is robust with profound physical insight. Utilization of such descriptor provides a simple “phase diagram” which enable us to quickly screen all the possible TIs in the tetradymite family with arbitrary mutation of atoms and stoichiometry. Moreover, the underlying design principle can be readily generalized to find new possible TIs containing the remaining group-VA (N, P) and group-VIA elements (O, Po), and even group-VB (V, Nb, Ta) and group-VIB (Cr, Mo, W) elements.

2. Methodology

To identify the topological nature of the training data of 230 tetradymites, we have performed first-principles calculations within the framework of density-functional theory (DFT) by using the projector-augmented wave (PAW) method [43, 44]. The code is implemented in the Vienna *ab-initio* simulation package (VASP). The exchange-correlation functional is treated using Perdew–Burke–Ernzerhof (PBE) with

generalized gradient approximation (GGA) [45]. The plane-wave basis with an energy cutoff of 500 eV is used and a $11 \times 11 \times 11$ Monkhorst-Pack k mesh [46] is adopted for the Brillouin zone integrations. The van der Waals (vdW) interaction is explicitly included in our calculations by adopting appropriate functionals [47-49]. The spin-orbit coupling (SOC) effect is taken into account to calculate the electronic band structure, and the Z_2 invariants are obtained by using Wilson loop as implemented in the software package WannierTools [50].

The compressed-sensing technique [38] is then adopted to find a physically interpretable descriptor which can effectively classify the TIs and NIs among the training data. In general, such an approach includes two main steps for machine learning. The first one is feature space construction. Through appropriate algebraic/functional operations $\{I, +, -, \times, /, \exp, \log, | \cdot |, \sqrt{\cdot}, ^{-1}, ^2, ^3\}$ between all the available combinations of primary features (e.g., the atomic number, the electronegativity, the ionization energy, the affinity energy and etc.) up to a certain complexity cutoff (number of applied operators), the feature space is formed by n vectors $D_n = (D_{n,1}, D_{n,2}, \dots, D_{n,m})$, where $D_{n,m}$ is the n^{th} potential descriptor, evaluated on the m^{th} sample. More details on the feature space construction can be found in References [38, 51]. The second step is descriptor identification which includes the combination of SIS (sure independence screening) and SO (sparsifying operators). Here SIS selects the subspace containing the features highly relevant on target material property. After the reduction of ultrahigh dimensional feature space, the l_0 -norm regularized minimization is adopted to pinpoint the optimal n -dimensional descriptor in SO. The leave-one-out cross-validation is then used to evaluate the performance of classification algorithms.

3. Results and discussion

As mentioned above, the training data of 230 tetradymite compounds can be obtained by possible mutations of cations (As, Sb and Bi) and anions (S, Se and Te). In principle, the resulting system can be binary, ternary, quaternary, quintuple or even

hexahydroxy. As an example, Figure 1 shows the crystal structure of a quintuple tetradymite SbBiSeTeS , where the atoms Sb, Bi, Se, Te, S occupy the sites A, B, C, D, E, respectively. The system can be viewed as stacking the so-called quintuple layers (QLs) through the vdW interactions. In the present work, the vdW functional in the form of optB86b [48, 47, 52, 53] is found to accurately reproduce the experimentally measured lattice parameters of several tetradymites. To identify the topological nature of quintuple SbBiSeTeS , we first calculate its orbital-decomposed band structure. As can be seen from Figure S1 of the supplementary materials (SM), the highest valence band (HVB) at the Γ point are mainly occupied by the p_z orbitals of Bi and Sb atoms, while the lowest conduction band (LCB) by the p_z orbital of Te atom. Such band inversion behavior is very similar to that found in the topological nontrivial Bi_2Te_3 [9]. As can be seen from the corresponding evolution lines of Wannier centers (see Figure S1), the Z_2 invariant is calculated to be (1;000) indicating that the quintuple SbBiSeTeS is indeed a strong TI. Similar calculations have been done for all the other tetradymites, and the results indicate that there are 67 TIs and 163 NIs among the 230 training data.

In order to find an effective descriptor to classify the above-mentioned TIs and NIs, we first construct the feature space by selecting appropriate input variables such as the atomic number, the electronegativity, the ionization energy, and the affinity energy of all the constituent atoms A, B, C, D, E. Extensive test calculations indicate that a better descriptor can be found with only two kinds of variables, namely, the atomic number (Z_A, Z_B, Z_C, Z_D, Z_E) and the electronegativity ($\chi_A, \chi_B, \chi_C, \chi_D, \chi_E$). Using these 10 primary features, a pool of about 10^7 different combined features is initially developed and further reduced to 50000 after screening by SIS. Finally, the SO is adopted to pinpoint the optimized descriptors for our investigated 230 training data, which is 2D in nature and given by

$$D_1 = \frac{1}{\chi_E \left(\frac{1}{Z_B Z_C} + \frac{1}{Z_A Z_D} \right)}, \quad (1)$$

$$D_2 = |(\chi_C - \chi_E)|Z_B - Z_D| + (Z_A - Z_C)|\chi_D - \chi_E||, \quad (2)$$

If D_1 and D_2 are respectively denoted as the x and y coordinates, we plot a “phase diagram” of the 230 tetradymites shown in Figure 2, where the blue and green areas are determined by connecting the outermost black points (163 NIs) and red points (67 TIs), respectively. Generally speaking, a candidate tetradymite would exhibit TI nature if it has a larger D_1 value. This is reasonable since heavy atoms (larger Z_A, Z_B, Z_C, Z_D , or smaller χ_E) usually have larger SOC strength which is very important to drive the TI nature. For example, the well-known TI Bi_2Te_3 exhibits the maximum D_1 value of 1018 among all the 230 tetradymites, since it has the largest atomic number of both the cations and anions ($Z_A=Z_B=83, Z_C=Z_D=52$) together with the smallest electronegativity of the anion in site E ($\chi_E=2.12$). If we focus on the region with $336 < D_1 < 426$, we find that a system with smaller D_2 value tends to fall into the TI area. To have a better understanding of the underlying physical mechanism, we rewrite Equation (2) as

$$D_2 = \left| \left((\chi_C - \chi_B) + (\chi_B - \chi_E) \right) |Z_B - Z_D| + (Z_A - Z_C) \left| (\chi_D - \chi_A) + (\chi_A - \chi_E) \right| \right|, \quad (3)$$

where we see smaller electronegativity difference between the cations and anions (e.g., $(\chi_C - \chi_B), (\chi_B - \chi_E), (\chi_D - \chi_A), (\chi_A - \chi_E)$) can lead to a lower D_2 value. According to previous analysis [54], a candidate compound is likely to exhibit topologically non-trivial nature if it has small electronegativity difference between the cations and anions. Otherwise, the system tends to be a NI, as also evidenced by relatively higher D_2 value of the blue area. It should be noted that a moderate D_1 value in the range of 336~426 means that the atomic number of Z_A, Z_B, Z_C , and Z_D should not be large or small simultaneously. In particular, if the cations (A and B) and the anions (C and D) are “diagonally” selected from the periodical table, the resulting tetradymite must have the largest $(Z_B - Z_D)$ and $(Z_A - Z_C)$ values, which leads to a higher D_2 value and thus the system tends to be in the NI area. The physical mechanism is similar to the above discussion since large atomic number difference between cations and anions also causes large electronegativity difference. Taking

Bi₂TeS₂ (also denoted as Bi-Bi-Te-S-S in accordance with the A, B, C, D, E sites) as an example, there exist large differences in both the atomic number and the electronegativity between the cations (Bi) and the anions (Te and S). As a consequence, a moderate D_1 value of 394 with a high D_2 value of 31 can be found according to Eq. (1) and (3), respectively. That is, the Bi₂TeS₂ should appear in the NI area of the phase diagram, which is also confirmed by our first-principles calculations (see Figure S2 of SM). We have also done leave-one-out cross-validation to check the learning performance of the proposed descriptor. Namely, one sample is randomly removed from 230 and the left 229 are used as new training data to reconstruct appropriate classification descriptors. Extensive learning tests suggest that the above-mentioned 2D descriptor (Eq. 1 and 2) always appears in the top 10 candidates, which indicates it is very robust with profound physical insight. It is noted that there is only a small overlap between the NI and TI domains in Fig. 2, which yields a high accuracy of ~97% of the proposed descriptor. To sum up, the optimized 2D descriptor (D_1 , D_2) can not only capture the fundamental driven nature of TIs, but also enable us to draw a phase diagram from which all the potential TIs in the tetradymite family can be quickly predicted.

Up to now, all the 230 tetradymites in the training data have a particular integer stoichiometry with nominal formula of ABCDE. In the experiments, however, most of the samples may have arbitrary fractional stoichiometry, such as ternary tetradymite Bi₂Te_{3-x}S_x with $x = 0 \sim 0.12$ [55], quaternary tetradymite Bi_{1.5}Sb_{0.5}Te_{1.3}Se_{1.7} and Bi_{1.4}Sb_{0.6}Te_{1.8}S_{1.2} [56, 57]. In general, one can use a unique formula of As_xSb_yBi_{2-x-y}S_xSe_yTe_{3-x-y} to represent a tetradymite with arbitrary mutation of atoms and stoichiometry. It is interesting to check whether such “complicated” systems are TI or NI, which is however impossible from first-principles approach since prohibitively large supercell is needed. Such an issue can be readily addressed by utilization of our proposed 2D descriptor if we define five weighted atomic numbers

$$Z_A = x_1 Z_{As} + y_1 Z_{Sb} + (1 - x_1 - y_1) Z_{Bi} \quad , \quad Z_B = x_2 Z_{As} + y_2 Z_{Sb} + (1 - x_2 - y_2) Z_{Bi} \quad ,$$

$Z_C = x_3 Z_S + y_3 Z_{Se} + (1 - x_3 - y_3) Z_{Te}$, $Z_D = x_4 Z_S + y_4 Z_{Se} + (1 - x_4 - y_4) Z_{Te}$,
 $Z_E = x_5 Z_S + y_5 Z_{Se} + (1 - x_5 - y_5) Z_{Te}$, and five weighted electronegativity
 $\chi_A = x_1 \chi_{As} + y_1 \chi_{Sb} + (1 - x_1 - y_1) \chi_{Bi}$, $\chi_B = x_2 \chi_{As} + y_2 \chi_{Sb} + (1 - x_2 - y_2) \chi_{Bi}$,
 $\chi_C = x_3 \chi_S + y_3 \chi_{Se} + (1 - x_3 - y_3) \chi_{Te}$, $\chi_D = x_4 \chi_S + y_4 \chi_{Se} + (1 - x_4 - y_4) \chi_{Te}$,
 $\chi_E = x_5 \chi_S + y_5 \chi_{Se} + (1 - x_5 - y_5) \chi_{Te}$, where $x_1, x_2, x_3, x_4, x_5, y_1, y_2, y_3, y_4, y_5$ change
 from 0 to 1 with an interval of 0.2. Inserting these variables into Eq. (1) and (2), a
 total of $\sim 4 \times 10^6$ (D_1, D_2) pairs at arbitrary stoichiometry $As_x Sb_y Bi_{2-x-y} S_x Se_{y'} Te_{3-x'-y'}$
 ($x = x_1 + x_2, y = y_1 + y_2, x' = x_3 + x_4 + x_5, y' = y_3 + y_4 + y_5$) is obtained and then
 mapped into the phase diagram. As illustrated in Figure 3, a larger number of new
 tetradymites appeared in the green area are quickly predicted to be potential TIs. As a
 testing example, if $x = 0, y = 0, x' = 1.4$ and $y' = 0$, we have a ternary tetradymite
 $Bi_2 Te_{1.6} S_{1.4}$ with $D_1 = 702$ and $D_2 = 12$. As shown in Figure 3, this particular ($D_1,$
 D_2) point is located at the TI area, which agrees well with the experimental fact that
 $Bi_2 Te_{1.6} S_{1.4}$ exhibit obvious topologically-nontrivial nature [58]. Once again, these
 findings demonstrate that the 2D descriptor is indeed an effective tool to quickly
 screen new TI candidates in the tetradymite family and in turn provides useful
 guidance for the related experiments.

To show that the proposed 2D descriptor is transferable, we first consider the case
 where more elements from the group-VA (N, P) and group-VIA (O, Po) are included
 to construct the tetradymites structure. Hence, a total of 3125 candidates (including
 the original 230 typical tetradymites) are mapped into the phase diagram. As can be
 seen from Figure 4(a), many new compounds appear in the green area and could be
 potential TIs. In addition to those possible NIs in the blue area, we also observe many
 candidate systems falling outside the two phase areas. The possible reason is that we
 use a relatively smaller training data of 230 tetradymites with 6 typical component
 elements (As, Sb, Bi and S, Se, Te). To check the predictive power of the phase

diagram, we randomly chose one candidate (BiSbSeTePo) in the TI area. Additional first-principles calculations indicate that the LCB at the Γ point is mainly occupied by the p_z orbitals of the Se and Te atoms, while the HVB occupied by the p_x and p_y orbitals of Po atom (see Figure 4(b)). These findings suggest that the BiSbSeTePo compound exhibits obvious band inversion caused by the SOC. Moreover, the corresponding Z_2 invariant is calculated to be (1;000) which further confirms that BiSbSeTePo is a strong TI. On the other hand, we find that the proposed 2D descriptor and the phase diagram can be even generalized to predict possible TIs with constituent cations and anions from group-VB (V, Nb, Ta) and group-VIB (Cr, Mo, W). As indicated in Figure 5, the many candidate compounds appeared in the green area suggest that there is still room to find new TIs with tetradymite structure, which needs further theoretical and experimental investigations.

4. Conclusion

In conclusion, we overcome the formidable task of first-principles characterization by adopting a statistical-learning approach to predict all the possible TIs with tetradymite structure. As derived by the compressed sensing technique, an effective 2D descriptor is proposed which requires only the atomic number and electronegativity of the constituent elements. Such a machine-learned descriptor is physically interpretable with high accuracy and strong transferability. Most importantly, the utilization of the 2D descriptor provides a simple “phase diagram” by which one can quickly identify possible TIs with arbitrary mutation of atoms and/or stoichiometry.

Acknowledgments

We thank financial support from the National Natural Science Foundation (Grant Nos. 11574236 and 51772220). The numerical calculations in this work have been done on the platform in the Supercomputing Center of Wuhan University.

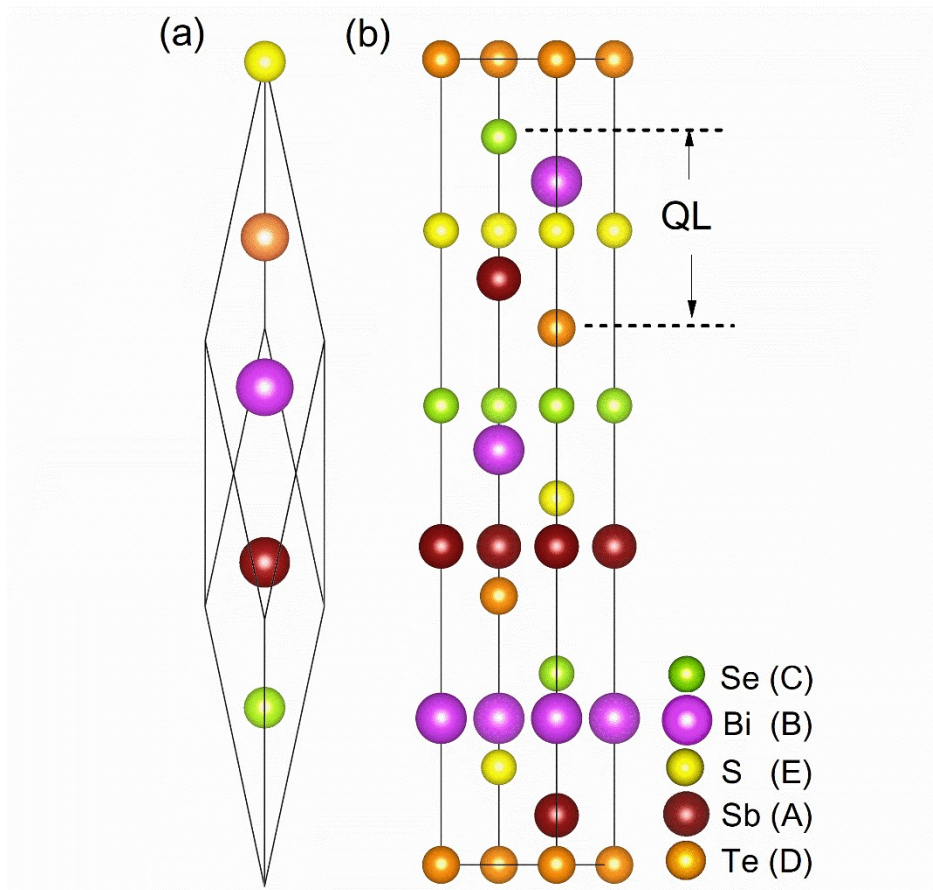


Figure 1. The crystal structure of an exempling quintuple tetradymites SbBiSeTeS , where (a) is the primitive cell, (b) is the unit cell, and the atoms Sb, Bi, Se, Te, S occupy the sites A, B, C, D, E, respectively.

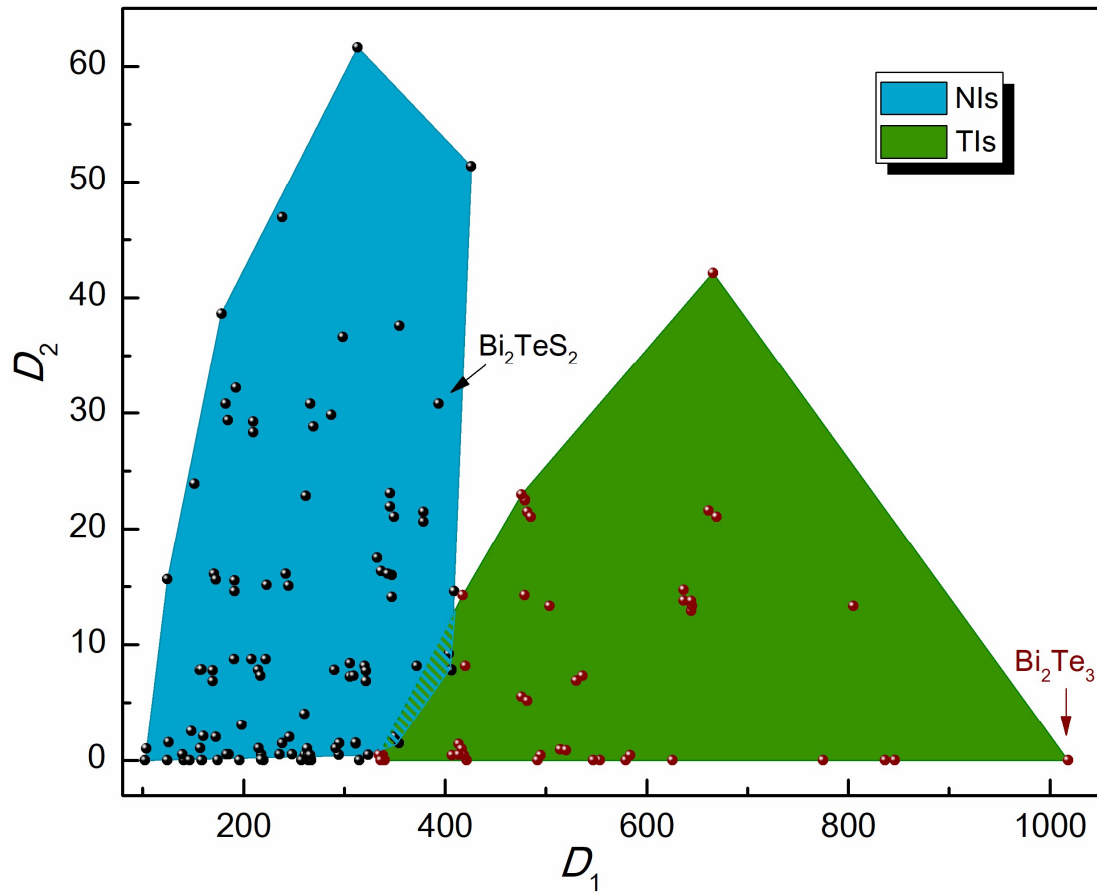


Figure 2. Phase diagram of the 230 training data defined by the 2D descriptor. NI and TI phases are respectively denoted as the blue and green areas, which are determined by connecting the outermost black points (163 NIs) and red points (67 TIs).

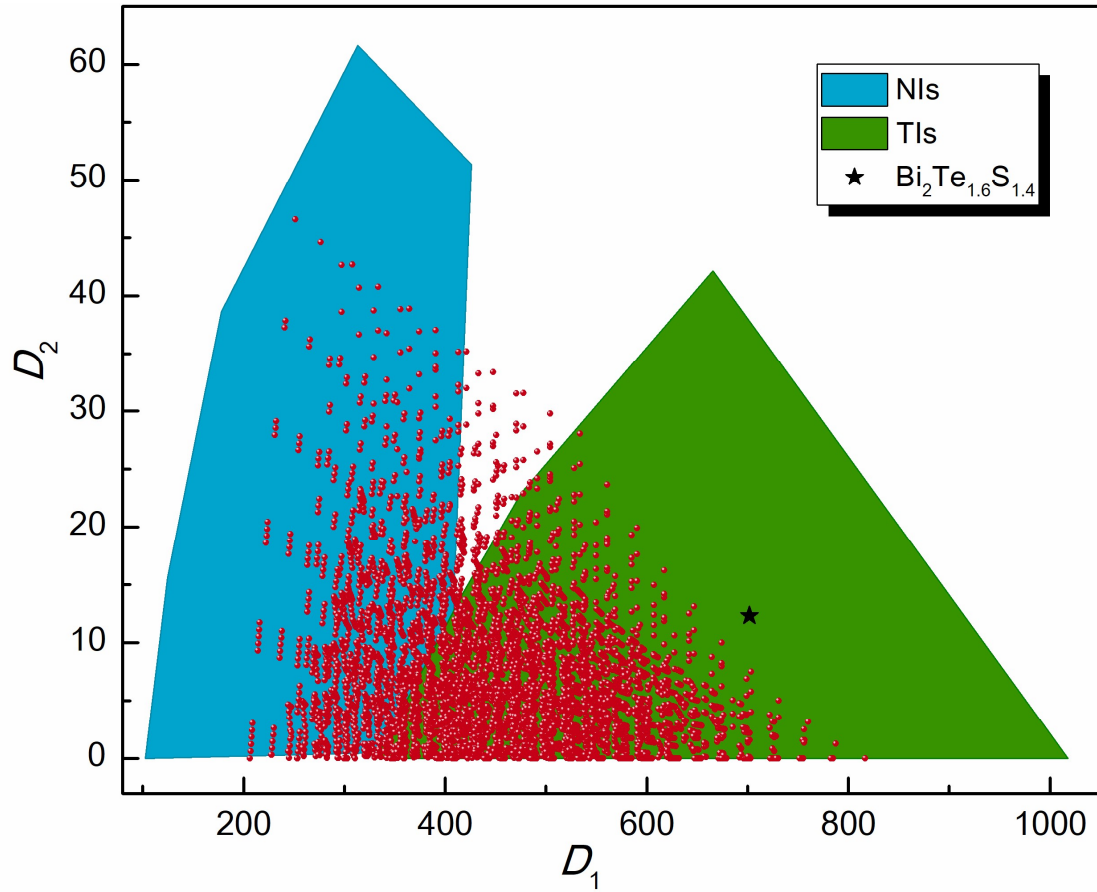


Figure 3. Possible tetradymites having arbitrary mutation of atoms and stoichiometry $\text{As}_x\text{Sb}_y\text{Bi}_{2-x-y}\text{S}_{x'}\text{Se}_{y'}\text{Te}_{3-x'-y'}$, mapped into the phase diagram according to the calculated (D_1, D_2) values. Note here $x = x_1 + x_2$, $y = y_1 + y_2$, $x' = x_3 + x_4 + x_5$, $y' = y_3 + y_4 + y_5$ and we choose $x_1 = x_2 = y_1 = y_2 = 0.2$ for simplicity. The asterisk indicated in the green area indicates a particular tetradymites $\text{Bi}_2\text{Te}_{1.6}\text{S}_{1.4}$.

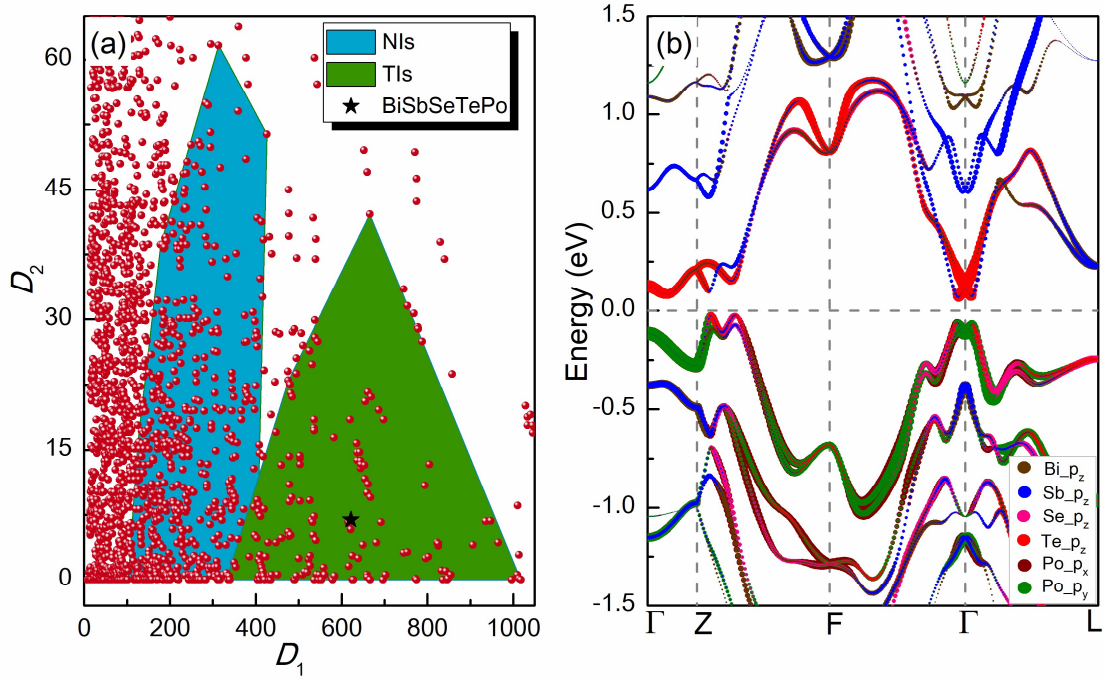


Figure 4. (a) Possible tetradymites with additional elements from group-VA (N, P) and group-VIA (O, Po), mapped into the phase diagram according to their calculated (D_1 , D_2) values. (b) The orbital-decomposed band structure of BiSbSeTePo (marked by asterisk in (a)). The colored circles represent the orbital compositions, and the sizes of the circles are proportional to their contributions.

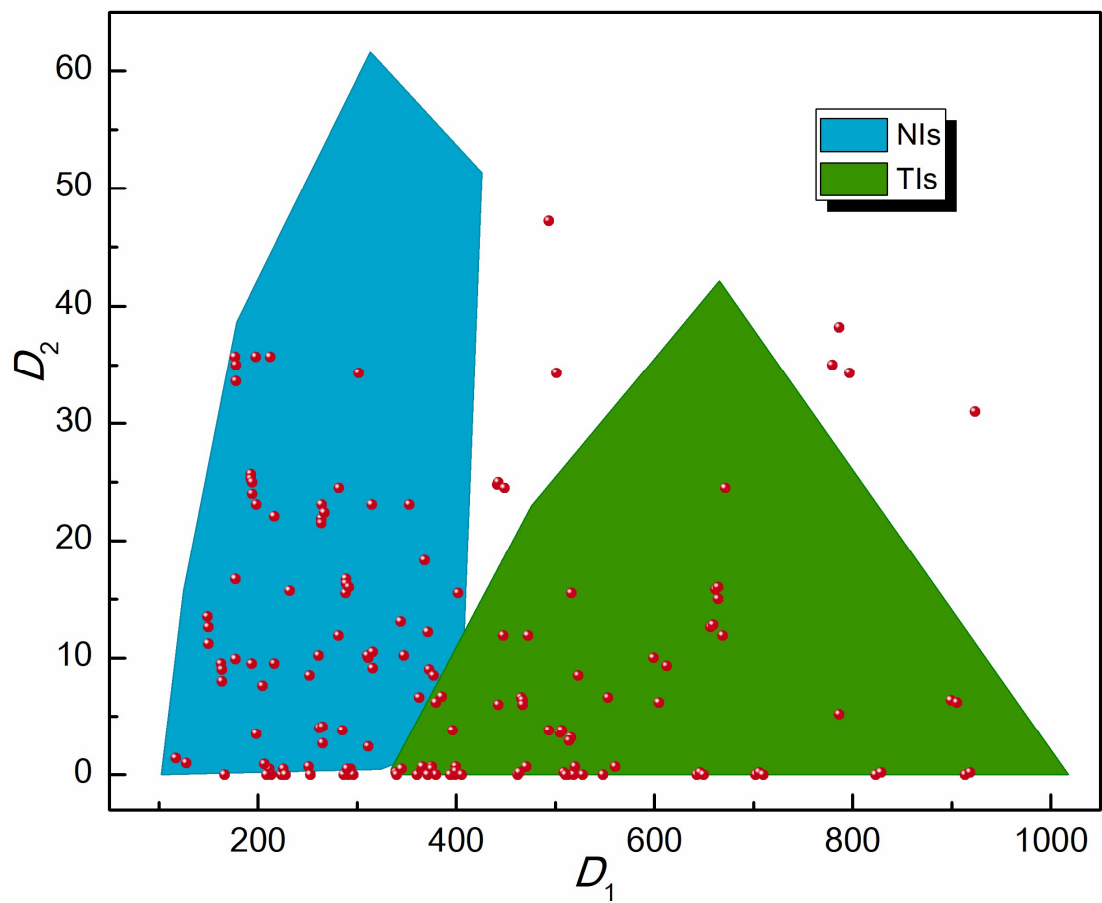


Figure 5. Possible tetradymites with constituent atoms from group-VB (V, Nb, Ta) and group-VIB (Cr, Mo, W), mapped into the phase diagram according to their calculated (D_1 , D_2) values.

References

- [1] X. L. Qi and S. C. Zhang, *Phys. Today* **63**, 33 (2010).
- [2] M. Z. Hasan and C. L. Kane, *Rev. Mod. Phys.* **82**, 3045 (2010).
- [3] D. Pesin and A. H. MacDonald, *Nat. Mater.* **11**, 409–416 (2012).
- [4] C. Brüne, A. Roth, H. Buhmann, E. M. Hankiewicz, L. W. Molenkamp, J. Maciejko, X.-L. Qi, and S.-C. Zhang, *Nat. Phys.* **8**, 486–490 (2012).
- [5] J. Wunderlich, B. G. Park, A. C. Irvine, L. P. Zárbo, E. Rozkotová, P. Nemeč, V. Novák, J. Sinova, and T. Jungwirth, *Science* **330**, 1801–1804 (2010).
- [6] F. Mahfouzi, N. Nagaosa, and B. K. Nikolić, *Phys. Rev. Lett.* **109**, 166602 (2012).
- [7] C. H. Li, O. M. van't Erve, J. T. Robinson, Y. Liu, L. Li, and B. T. Jonker, *Nat. Nanotechnol.* **9**, 218–224 (2014).
- [8] A. R. Mellnik, J. S. Lee, A. Richardella, J. L. Grab, P. J. Mintun, M. H. Fischer, A. Vaezi, A. Manchon, E. A. Kim, N. Samarth, and D. C. Ralph, *Nature* **511**, 449–451 (2014).
- [9] H. J. Zhang, C.-X. Liu, X.-L. Qi, X. Dai, Z. Fang, and S.-C. Zhang, *Nat. Phys.* **5**, 438–442 (2009).
- [10] D. Hsieh, Y. Xia, D. Qian, L. Wray, F. Meier, J. H. Dil, J. Osterwalder, L. Patthey, A. V. Fedorov, H. Lin, A. Bansil, D. Grauer, Y. S. Hor, R. J. Cava, and M. Z. Hasan, *Phys. Rev. Lett.* **103**, 146401 (2009).
- [11] T. Sato, K. Segawa, H. Guo, K. Sugawara, S. Souma, T. Takahashi, and Y. Ando, *Phys. Rev. Lett.* **105**, 136802 (2010).
- [12] Y. L. Chen, Z. K. Liu, J. G. Analytis, J.-H. Chu, H. J. Zhang, B. H. Yan, S.-K. Mo, R. G. Moore, D. H. Lu, I. R. Fisher, S. C. Zhang, Z. Hussain, and Z.-X. Shen, *Phys. Rev. Lett.* **105**, 266401 (2010).
- [13] D. Takane, K. Nakayama, S. Souma, T. Wada, Y. Okamoto, K. Takenaka, Y. Yamakawa, A. Yamakage, T. Mitsuhashi, K. Horiba, H. Kumigashira, T. Takahashi, and T. Sato, *npj Quantum Mater.* **3**, 1 (2018).
- [14] E. Perim, D. Lee, Y. Liu, C. Toher, P. Gong, Y. Li, W. N. Simmons, O. Levy, J. J. Vlassak, J. Schroers, and S. Curtarolo, *Nat. Commun.* **7**, 12315 (2016).

-
- [15] L. Ward, A. Agrawal, A. Choudhary, and C. Wolverton *NPJ Comput. Mater.* **2**, 16028 (2016).
- [16] O. Isayev, C. Oses, C. Toher, E. Gossett, S. Curtarolo, and A. Tropsha, *Nat. Commun.* **8**, 15679 (2017).
- [17] K. Yang, W. Setyawan, S. Wang, M. Buongiorno Nardelli, and S. Curtarolo, *Nat. Mater.* **11**, 614–619 (2012).
- [18] H. C. Po, A. Vishwanath, and H. Watanabe, *Nat. Commun.* **8**, 50 (2017).
- [19] R. Sarmiento-Perez, T. F. Cerqueira, S. Korbelt, S. Botti, and M. A. Marques, *Chem. Mater.* **27**, 5957 (2015).
- [20] M. Klintenberg, J. Haraldsen, and A. Balatsky, *Appl. Phys. Res.* **6**, 31 (2014).
- [21] R. M. Geilhufe, A. Bouhon, S. S. Borysov, and A. V. Balatsky, *Phys. Rev. B* **95**, 041103(R) (2017)
- [22] L. Wang, *Phys. Rev. B* **94**, 195105 (2016).
- [23] G. Torlai and R. G. Melko, *Phys. Rev. B* **94**, 165134 (2016).
- [24] J. Carrasquilla and R. G. Melko, *Nat. Phys.* **13**, 431 (2017).
- [25] P. Broecker, J. Carrasquilla, R. G. Melko, and S. Trebst, *Sci. Rep.* **7**, 8823 (2017).
- [26] K. Ch'ng, J. Carrasquilla, R. G. Melko, and E. Khatami, *Phys. Rev. X* **7**, 031038 (2017).
- [27] L.-F. Arsenault, O. A. von Lilienfeld, and A. J. Millis, [arXiv:1506.08858](https://arxiv.org/abs/1506.08858).
- [28] Y. Zhang and E.-A. Kim, *Phys. Rev. Lett.* **118**, 216401 (2017).
- [29] Y. Zhang, R. G. Melko, and E.-A. Kim, *Phys. Rev. B* **96**, 245119 (2017).
- [30] D.-L. Deng, X. P. Li, and S. Das Sarma, *Phys. Rev. B* **96**, 195145 (2017).
- [31] P. F. Zhang, H. T. Shen, and H. Zhai, *Phys. Rev. Lett.* **120**, 066401 (2018).
- [32] D. Carvalho, N. A. García-Martínez, J. L. Lado, and J. Fernández-Rossier, *Phys. Rev. B* **97**, 115453 (2018).
- [33] R. Biswas, L. Blackburn, J. Cao, R. Essick, K. A. Hodge, E. Katsavounidis, K. Kim, Y.-M. Kim, E.-O. Le Bigot, C.-H. Lee, J. J. Oh, S. H. Oh, E. J. Son, Y. Tao, R. Vaulin, and X. Wang, *Phys. Rev. D* **88**, 062003 (2013).
- [34] B. P. Abbott et al. (LIGO Scientific Collaboration and Virgo Collaboration), *Phys.*

-
- [Rev. Lett. **116**, 061102 \(2016\).](#)
- [35] M. Pasquato, [arXiv:1606.08548](#).
- [36] Q. Zhou, P. Tang, S. Liu, J. Pan, Q. Yan, and S. C. Zhang, [Proc. Natl. Acad. Sci. U.S.A. **201801181** \(2018\).](#)
- [37] L. M. Ghiringhelli, J. Vybiral, S. V. Levchenko, C. Draxl, and M. Scheffler, [Phys. Rev. Lett. **114**, 105503 \(2015\).](#)
- [38] R. Ouyang, S. Curtarolo, E. Ahmetcik, M. Scheffler, and L. M. Ghiringhelli, [arXiv:1710.03319 \(2017\).](#)
- [39] J. Reimann, J. Gdde, K. Kuroda, E. V. Chulkov, and U. Hfer, [Phys. Rev. B **90**, 081106\(R\) \(2014\).](#)
- [40] D. Kong, Y. Chen, J. J. Cha, Q. Zhang, J. G. Analytis, K. Lai, Z. Liu, S. Sae Hong, K. J. Koski, S.-K. Mo, Z. Hussain, I. R. Fisher, Z.-X. Shen, and Y. Cui, [Nat. Nanotechnol. **6**, 705–709 \(2011\).](#)
- [41] C.-K. Lee, C.-M. Cheng, S.-C. Weng, W.-C. Chen, K.-D. Tsuei, S.-H. Yu, M. M.-C. Chou, C.-W. Chang, L.-W. Tu, H.-D. Yang, C.-W. Luo, and M. M. Gospodinov, [Sci. Rep. **6**, 36538 \(2016\).](#)
- [42] G. L. Hao, X. Qi, L. Xue, C. Y. Cai, J. Li, X. L. Wei, and J. X. Zhong, [J. Appl. Phys. **113**, 024306 \(2013\).](#)
- [43] P. E. Blchl, [Phys. Rev. B **50**, 17953 \(1994\).](#)
- [44] G. Kresse and D. Joubert, [Phys. Rev. B **59**, 1758 \(1999\).](#)
- [45] J. P. Perdew, K. Burke, and M. Ernzerhof, [Phys. Rev. Lett. **77**, 3865 \(1996\).](#)
- [46] D. J. Chadi, and M. L. Cohen, [Phys. Rev. B **8**, 5747 \(1973\).](#)
- [47] T. Thonhauser, V. R. Cooper, S. Li, A. Puzder, P. Hyldgaard, and D. C. Langreth, [Phys. Rev. B **76**, 125112 \(2007\).](#)
- [48] J. Klimeš, D. R. Bowler, and A. Michaelides, [J. Phys.: Condens. Matter **22**, 022201 \(2009\).](#)
- [49] J. Klimeš, D. R. Bowler, and A. Michaelides, [Phys. Rev. B **83**, 195131 \(2011\).](#)
- [50] Q. Wu, S. Zhang, H.-F. Song, M. Troyer and A. A. Soluyanov, [Comput. Phys. Commun. **224**, 405–416 \(2018\).](#)

-
- [51] L. M Ghiringhelli, J. Vybiral, E. Ahmetsik, R. Ouyang, S. V Levchenko¹, C. Drax, and M. Scheffler, [New. J. Phys. **19**, 023017 \(2017\)](#).
- [52] L. Cheng, H. J. Liu, J. Zhang, J. Wei, J. H. Liang, J. Shi, and X. F. Tang, [Phys. Rev. B **90**, 085118 \(2014\)](#).
- [53] G. H. Cao, H. J. Liu, J. H. Liang, L. Cheng, D. D. Fan, and Z. Y. Zhang, [Phys. Rev. B **97**, 075147 \(2018\)](#).
- [54] G. H. Cao, H. J. Liu, X.-Q. Chen, Y. Sun, J. H. Liang, R. Yu, and Z. Y. Zhang, [Sci. Bull. **62**, 1649–1653 \(2017\)](#).
- [55] J. Horak, P. Lostak, L. Koudelka, and R. Novotni, [Solid State Commun. **55**, 1031 \(1985\)](#).
- [56] Z. Ren, A. A. Taskin, S. Sasaki, K. Segawa, and Y. Ando, [Phys. Rev. B **84**, 165311 \(2011\)](#).
- [57] J. Huiwen, J. M. Allred, M. K. Fuccillo, M. E. Charles, M. Neupane, L. A. Wray, M. Z. Hasan, and R. J. Cava, [Phys. Rev. B **85**, 201103\(R\) \(2012\)](#).
- [58] H. Ji, J. M. Allred, M. K. Fuccillo, M. E. Charles, M. Neupane, L. A. Wray, M. Z. Hasan, and R. J. Cava, [Phys. Rev. B **85**, 201103\(2012\)](#).